Computational Mechanics (1988) 3, 381–397

Computational Mechanics

Modeling mixed-mode dynamic crack propagation using finite elements: Theory and applications

D. V. Swenson
Mechanical Engineering Department, Kansas State University, Manhattan, Kansas 66506, USA

A. R. Ingraffea
Department of Civil and Environmental Engineering, Cornell University, Ithaca, NY 14853, USA

Abstract. Previous work in modeling dynamic fracture has assumed the crack will propagate along predefined mesh lines (usually a straight line). In this paper we present a finite element model of mixed-mode dynamic crack propagation in which this constraint is removed. Applying linear elasto-dynamic fracture mechanics concepts, discrete cracks are allowed to propagate through the mesh in arbitrary directions. The fracture criteria used for propagation and the algorithms used for remeshing are described in detail. Important features of the implementation are the use of triangular elements with quadratic shape functions, explicit time integration, and interactive computer graphics. These combine to make the approach robust and applicable to a broad range of problems.

Example analyses of straight and curving crack problems are presented. Verification problems include a stationary crack under dynamic loading and a propagating crack in an infinite body. Comparisons with experimental data are made for curving propagation in a cracked plate under biaxial loading.

1 Introduction

Dynamic fracture deals with fracture under conditions where inertia must be included in the problem formulation. This occurs either under dynamic loading or in the case of static loading as a rapidly propagating crack runs through a structure. In mixed-mode propagtion the crack is not confined to propagate in a straight line but may curve under the influence of asymmetric loading.

Since Yoffe's (1951) analysis of a fixed length crack moving across a plate, analytical solutions have been obtained for several specific crack propagation problems. Among these are Broberg's (1960) crack starting from zero length and extending at constant velocity and Nilsson's (1972) semi-infinite crack propagating at constant velocity in a strip. (See Sih and Chen (1977) for a more comprehensive compilation.)

Freund (1972a, b; 1973, 1974) developed the general solution for a cracked infinite body initially in static equilibrium. At a certain instant, the crack begins to move. A main result of his analysis is a relation between the dynamic stress intensity and the initial static condition

$$K = k(v) K_S(a), \tag{1}$$

where K is the dynamic stress intensity, $k(v)$ is a universal function of crack velocity (v) and material properties, and $K_S(a)$ is the static stress intensity obtained at the current crack length (a) using the initial static stresses in the body as loads on the crack face. The universal function, $k(v)$, has a value of one at zero crack velocity, and a value of zero at the Rayleigh wave speed, c_R. Freund also proves that the solution for a crack with non-uniform velocity can be developed as the limit of a series of time increments, with constant velocities in each increment.

Although specific analytic solutions are useful, solutions for general problems can only be obtained using numerical techniques (usually finite element or finite difference methods). Some of the numerical approaches include work by Kobayashi, Emery, and Mall (1976) where nodal release is used to model crack propagation; the analysis by Jung, Ahmed, Kanninen, and Popelar (1981), also using nodal release; the use of a translating singularity element by Nishioka and Atluri (1980a, b); and the finite difference work of Chen and Wilkins (1977). Additional recent work on

dynamic fracture includes that of Koh and Haber (1986) using a mixed Eulerian-Lagrangian model and that of Valliapan and Murti (1985) using quarter-point elements at the crack tip. A summary of numerical methods is given in a paper by Atluri and Nishioka (1985). In all these cases, the crack has been constrained to propagate in directions specified a priori.

The remainder of this paper is divided into five sections. In Sect. 2 the solution for stresses, displacements, and velocities around a moving crack will be discussed. In Sect. 3 the finite element approximation will be summarized. The implementation of these concepts will be shown in Sect. 4. In Sect. 5 we compare numerical results with analytical solutions for stationary and moving cracks, and in Sect. 6 we present the application of the model to biaxial loading experiments.

2 Dynamic linear elastic fracture mechanics

2.1 Asymptotic solution

In this work, dynamic fracture will be approach in a manner analogous to that used in static linear elastic fracture mechanics. The asymptotic solution for stresses, velocities, and displacements around the crack tip will be given in terms of stress intensity factors and the current crack velocity.

There are several approaches to obtaining the displacement and stresses around a moving crack, including use of a complex stress function (Radok 1956) or asymptotic arguments (Freund and Clifton 1974). Alternately, we can develop the solution without using complex functions by looking for the steady state solution with respect to coordinates (x,y) moving at the crack tip (1986). As shown by Achenbach and Bazant (1975) and by Freund and Clifton (1974), this solution is also valid for transient cracks in the limit as $r \to 0$. The following relations are then obtained for the displacements, velocities, and stresses around a moving crack (X, Y, and Z are stationary coordinates, v is the crack velocity).

For Mode I,

$$u_X = \frac{K_I}{\mu}\frac{\sqrt{2}}{\sqrt{\pi}} H\left[(\beta_2^2+1)\sqrt{\beta_1 r_1}\cos\frac{\theta_1}{2} - 2\beta_1\beta_2\sqrt{\beta_2 r_2}\cos\frac{\theta_2}{2}\right]$$

$$u_Y = \frac{K_I}{\mu}\frac{\sqrt{2}}{\sqrt{\pi}} H\left[-\beta_1(\beta_2^2+1)\sqrt{\beta_1 r_1}\sin\frac{\theta_1}{2} + 2\beta_1\sqrt{\beta_2 r_2}\sin\frac{\theta_2}{2}\right]$$

$$\dot{u}_X = \frac{vK_I}{\mu\sqrt{2\pi}} H\left[-(\beta_2^2+1)\frac{1}{\sqrt{\beta_1 r_1}}\cos\frac{\theta_1}{2} + 2\beta_1\beta_2\frac{1}{\sqrt{\beta_2 r_2}}\cos\frac{\theta_2}{2}\right]$$

$$\dot{u}_Y = \frac{vK_I}{\mu\sqrt{2\pi}} H\left[-\beta_1(\beta_2^2+1)\frac{1}{\sqrt{\beta_1 r_1}}\sin\frac{\theta_1}{2} + 2\beta_1\frac{1}{\sqrt{\beta_2 r_2}}\sin\frac{\theta_2}{2}\right]$$

$$\sigma_{XX} = \frac{K_I}{\sqrt{2\pi}} H\left[(\beta_2^2+1)(2\beta_1^2-\beta_2^2+1)\frac{1}{\sqrt{\beta_1 r_1}}\cos\frac{\theta_1}{2} - 4\beta_1\beta_2\frac{1}{\sqrt{\beta_2 r_2}}\cos\frac{\theta_2}{2}\right]$$

$$\sigma_{YY} = \frac{K_I}{\sqrt{2\pi}} H\left[-(\beta_2^2+1)^2\frac{1}{\sqrt{\beta_1 r_1}}\cos\frac{\theta_1}{2} + 4\beta_1\beta_2\frac{1}{\sqrt{\beta_2 r_2}}\cos\frac{\theta_2}{2}\right]$$

$$\sigma_{XY} = \frac{K_I}{\sqrt{2\pi}} H\left[2\beta_1(\beta_2^2+1)\frac{1}{\sqrt{\beta_1 r_1}}\sin\frac{\theta_1}{2} - 2\beta_1(\beta_2^2+1)\frac{1}{\sqrt{\beta_2 r_2}}\sin\frac{\theta_2}{2}\right], \tag{2}$$

where, $H = \dfrac{1}{(4\beta_1\beta_2 - (\beta_2^2+1)^2)}$; $\quad \beta_1 = (1 - v^2/c_1^2)^{1/2}$; $\quad \beta_2 = (1 - v^2/c_2^2)^{1/2}$;

$x_1 = x/\beta_1$; $\quad y_1 = y$; $\quad x_2 = x/\beta_2$; $\quad y_2 = y$.

For Mode *II*,

$$u_X = \frac{K_{II}}{\mu}\frac{\sqrt{2}}{\sqrt{\pi}} H\left[2\beta_2\sqrt{\beta_1 r_1}\sin\frac{\theta_1}{2} - (\beta_2^2+1)\beta_2\sqrt{\beta_2 r_2}\sin\frac{\theta_2}{2}\right]$$

$$u_Y = \frac{K_{II}}{\mu}\frac{\sqrt{2}}{\sqrt{\pi}} H\left[2\beta_1\beta_2\sqrt{\beta_1 r_1}\sin\frac{\theta_1}{2} - (\beta_2^2+1)\sqrt{\beta_2 r_2}\cos\frac{\theta_2}{2}\right]$$

$$\dot{u}_X = \frac{v K_{II}}{\mu\sqrt{2\pi}} H\left[2\beta_2\frac{1}{\sqrt{\beta_1 r_1}}\sin\frac{\theta_1}{2} - (\beta_2^2+1)\beta_2\frac{1}{\sqrt{\beta_2 r_2}}\sin\frac{\theta_2}{2}\right]$$

$$\dot{u}_Y = \frac{v K_{II}}{\mu\sqrt{2\pi}} H\left[-2\beta_1\beta_2\frac{1}{\sqrt{\beta_1 r_1}}\cos\frac{\theta_1}{2} + (\beta_2^2+1)\frac{1}{\sqrt{\beta_2 r_2}}\cos\frac{\theta_2}{2}\right]$$

$$\sigma_{XX} = \frac{K_{II}}{\sqrt{2\pi}} H\left[2\beta_2(\beta_2^2-1-2\beta_1^2)\frac{1}{\sqrt{\beta_1 r_1}}\sin\frac{\theta_1}{2} + 2\beta_2(\beta_2^2+1)\frac{1}{\sqrt{\beta_2 r_2}}\cos\frac{\theta_2}{2}\right]$$

$$\sigma_{YY} = \frac{K_{II}}{\sqrt{2\pi}} H\left[2\beta_2(\beta_2^2+1)\frac{1}{\sqrt{\beta_1 r_1}}\sin\frac{\theta_1}{2} - 2\beta_2(\beta_2^2+1)\frac{1}{\sqrt{\beta_2 r_2}}\sin\frac{\theta_2}{2}\right]$$

$$\sigma_{XY} = \frac{K_{II}}{\sqrt{2\pi}} H\left[4\beta_1\beta_2\frac{1}{\sqrt{\beta_1 r_1}}\cos\frac{\theta_1}{2} - (\beta_2^2+1)^2\frac{1}{\sqrt{\beta_2 r_2}}\cos\frac{\theta_2}{2}\right]. \tag{3}$$

For Mode *III*,

$$u_Z = K_{III}\frac{\sqrt{2}}{\sqrt{\pi}}\frac{\sqrt{r_2}}{\sqrt{\beta_2}}\sin(\theta_2/2)$$

$$\dot{u}_Z = \frac{v K_{III}}{\mu\beta_2}\frac{1}{\sqrt{2\pi}}\frac{1}{\sqrt{\beta_2 r_2}}\sin(\theta_2/2)$$

$$\sigma_{XZ} = \frac{-K_{III}}{\beta_2}\frac{1}{\sqrt{2\pi}}\frac{1}{\sqrt{\beta_2 r_2}}\sin(\theta_2/2)$$

$$\sigma_{XZ} = K_{III}\frac{1}{\sqrt{2\pi}}\frac{1}{\sqrt{\beta_2 r_2}}\cos(\theta_2/2)\,. \tag{4}$$

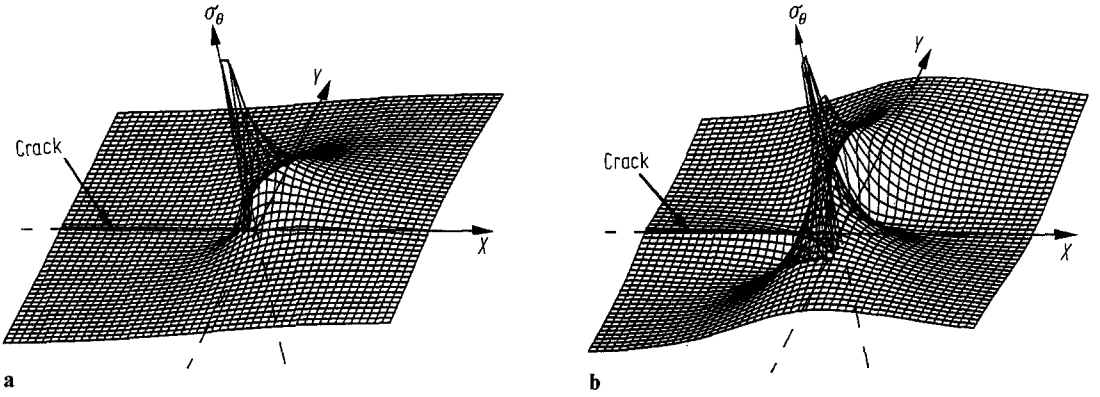

Fig. 1 a and b. Circumferential stresses around a mode *I* crack. **a** crack velocity zero; **b** crack velocity $0.99\,c_R$

The above stresses and displacements are the same as presented by Nishioka and Atluri (1983) (they did not include velocities).

The effect of crack velocity is illustrated in Fig. 1, which shows the circumferential stresses around a moving Mode *I* crack. In this figure, the circumferential stress is proportional to the height of the plotted surface above the X–Y plane. As noted by Yoffe, at a velocity of about 0.6 c_R the maximum stress at a constant radius no longer lies ahead of the crack, but has maxima off the crack axis.

These asymptotic equations provide the link between the finite element solution (which has a length scale the size of the elements) and the process zone (which has a much smaller length scale). We do not attempt to directly model the process zone, but assume that equal K fields imply equal fracture processes at the crack tip.

2.2 *Propagation criteria*

Given a fracture process described by the stress intensities and the crack velocity, it is necessary to formulate criteria to predict crack velocity and propagation direction. In this work, a curve relating crack velocity and critical stress intensity is used. Fig. 2 illustrates this curve for 4340 steel. The assumption of a unique curve was made for algorithmic convenience, it is not a necessary assumption. The initiation and arrest stress intensities are assumed to equal K_{ID} (or K_{IC}^d) at zero crack velocity. More complex relations could be used. All that is necessary is that, based on past history and the present state at the crack tip, a critical stress intensity for the current time is available.

An analogy can be made between the critical stress intensity curve and plasticity. Just as the stress remains on the yield surface during plastic straining, the stress intensity will lie on the $K_{ID}(v)$ curve during crack propagation. If the stress intensity is increasing, the crack velocity will increase. If the stress intensity is decreasing, the crack slows to remain on the curve. If the crack speed reaches zero, arrest has occurred.

In plasticity theory, a general stress state is often characterized by a scalar quantity for comparison with uniaxial material data. Similarly, in dynamic fracture the effects of K_I and K_{II} must be combined for comparison with $K_{ID}(v)$. The simplest way this can be done is by equating circumferential stresses. The maximum circumferential stress due to the combined K_I and K_{II} is calculated and compared to the value calculated using $K_{ID}(v)$ at the same crack velocity and radius. Because only the singular solution is used in this evaluation, the radial distance chosen for the evaluation does not affect the propagation criteria (Sect. 4.2).

The crack propagation direction also depends on the current stress intensities and crack velocity. There are at least three competing theories for predicting crack growth direction in mixed-mode static fracture: maximum circumferential stress, minimum strain energy density, and maximum

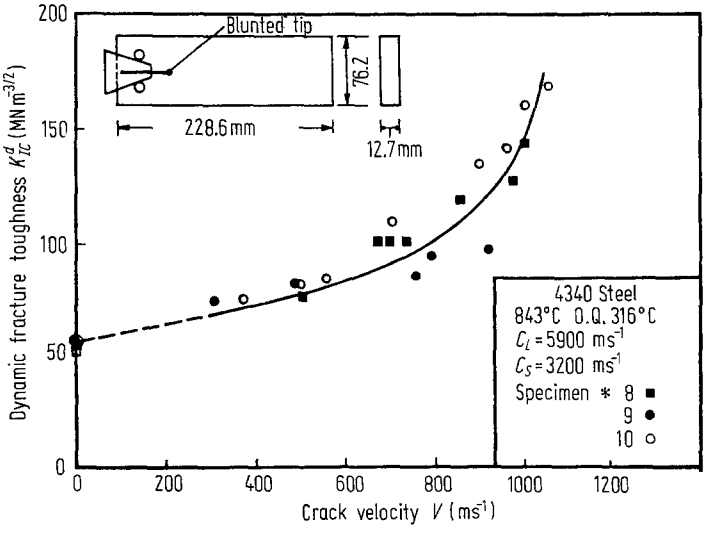

Fig. 2. Typical assumed $K_{ID}(v)$ curve (data for 4340 steel (Rosakis, Duffy, and Freund 1984)

energy release rate. Experience using the different theories in quasi-static analysis show that, from a practical standpoint, they are equivalent. The reason is that cracks curve in an attempt to propagate in Mode *I*. The same effect is seen in dynamic crack propagation experiments (Rossmanith 1983). Since the maximum circumferential stress criterion is easiest to implement and is intuitively reasonable, this method of predicting crack propagation direction was chosen.

3 Finite element approximation

In the finite element method, we divide the body into discrete elements, assume the form of displacements over each element, assemble the resulting global equations, and solve for the unknown accelerations. The accelerations are integrated in time to obtain velocities and displacements, developing a time history of the solution. The present approach closely follows that used by Key, Beisinger and Krieg in the HONDO code (1978). Since this approach has been used extensively, Bathe (1982) or Belytschko and Hughes (1983), only features pertinent to the present implementation will be mentioned.

The finite element approximation is obtained by assuming displacements are functions of the values at the nodes surrounding the element

$$\boldsymbol{u} = \mathbf{N}\boldsymbol{u}_a, \tag{5}$$

where $\boldsymbol{u}_a$ are the nodal displacements and $\mathbf{N}$ is a shape function matrix. Substituting this approximation into the weak statement of equilibrium and using the same interpolation functions for tractions gives,

$$\sum_{e=1}^{\text{Numel}} \left\{ \int_{S_{te}} \mathbf{N}^T\mathbf{N}\,\mathrm{d}S\,\boldsymbol{t}_a - \int_{V_e} \mathbf{B}^T\mathbf{D}\mathbf{B}\,\mathrm{d}V\,\boldsymbol{u}_a - \int_{V_e} \varrho\,\mathbf{N}^T\mathbf{N}\,\mathrm{d}V\,\ddot{\boldsymbol{u}}_a \right\} = \boldsymbol{0}. \tag{6}$$

where $\mathbf{D}$ relates the stresses to the strains, $\mathbf{B}$ relates strains to displacements, and $\boldsymbol{t}_a$ are surface tractions.

For the elements surrounding the crack tip (which is moving), the time derivative of Eq. (5) includes derivatives of the shape functions. These terms are functions of crack velocity and acceleration in combination with nodal velocities and displacements. Because of their pairing, these terms are small and have not been included in Eq. (6).

Assembling the element contributions, we obtain the global stiffness matrix ($\mathbf{K}$), the mass matrix ($\mathbf{M}$), and the load vector (f),

$$\mathbf{M}\ddot{\boldsymbol{u}}_a = \boldsymbol{f} - \mathbf{K}\boldsymbol{u}_a \tag{7}$$

We can now solve for the nodal accelerations,

$$\ddot{\boldsymbol{u}}_a = \mathbf{M}^{-1}(\boldsymbol{f} - \mathbf{K}\boldsymbol{u}_a). \tag{8}$$

If the mass matrix is diagonal, the inverse to obtain the accelerations is trivial. The following algorithm is used to evaluate Eq. (8) (note that the solution is obtained at the element level, no global matrices are actually assembled):

(1) Zero the force vector;

(2) Accumulate all external forces into this vectors;

(3) Loop through each element and add the internal forces to the external force vector;

(4) Calculate the current acceleration using the unbalanced nodal forces and the nodal masses.

The central difference scheme is used to integrate the accelerations. The velocity is assumed to be constant during a time increment. Using difference approximations for the velocities and accelerations, we obtain,

$$\ddot{\boldsymbol{u}}_n = \mathbf{M}^{-1}(\boldsymbol{f} - \mathbf{K}\boldsymbol{u}_n)$$

$$\dot{\boldsymbol{u}}_{n+1/2} = \dot{\boldsymbol{u}}_{n-1/2} + 1/2(\Delta t_{n-1/2} + \Delta t_{n+1/2})\ddot{\boldsymbol{u}}_n$$

$$\boldsymbol{u}_{n+1} = \boldsymbol{u}_n + \Delta t_{n+1/2}\dot{\boldsymbol{u}}_{n+1/2}, \tag{9}$$

where n indicates the time step.

This scheme uses the current state ($\boldsymbol{u}_n$, $\dot{\boldsymbol{u}}_{n-1/2}$) to obtain future velocities and displacements. Since no matrix inversion is necessary, the solution can be obtained for relatively large problems at many time steps within reasonable computational times. This makes it possible to use small time steps (also required for stability) and to follow stress waves in the structure. A second major advantage is that this approach places no requirements on the order in which nodes or elements are numbered, making it ideal for problems in which the mesh is changing during the course of the analysis. These two considerations make explicit time integration a natural choice for dynamic crack propagation.

The type of element must also be chosen. Three considerations lead to the use of the quadratic six-noded triangular element. A major consideration is incorporating the singular solution for displacements around the crack tip. This can be easily done by shifting the side nodes of the six-noded element to the quarter-point positions (Barsoum 1977; Henshell and Shaw 1975). A second consideration is the ease of automatically remeshing around the crack tip as the crack propagates. Meshes are generally easier to generate using triangular elements than quadrilateral elements. Finally, experience with the quadratic six-noded element has shown that it performs well in elastic analyses.

4 Implementation

4.1 Calculation of K_I and K_{II}

Given a finite element solution at an instant in time, several options are available to calculate K_I and K_{II}. These include the dynamic J integral, virtual crack extension, and fitting of the crack tip stresses or displacements to the asymptotic solution. It is desirable to calculate the stress intensities using parameters that are close to the crack tip so that rapid changes in stress intensity can be captured. Because of its ease of implementation and because it provides a local measure of crack tip response, the displacement correlation method is used. As implemented in its simplest form, nodal displacements on the crack face are used with Eqs. (2) and (3) to obtain the stress intensities.

4.2 Crack tip velocity and propagation direction

Incremental forms of the propagation criteria must be developed. The condition for crack initiation is,

$$\sigma_\theta^{\max} > \sigma_{\theta_D}^{\max} \tag{10}$$

where $\sigma_\theta^{\max}$ is the maximum circumferential stress calculated using the current stress intensities and crack velocities (zero for initiation) and $\sigma_{\theta_D}^{\max}$ is the circumferential stress using the critical stress intensity at the same crack velocity (the same radius is used in both calculations). This test is only made when the crack is stationary either because it has not propagated or because it has previously arrested.

If the crack is propagating, the difference between the maximum circumferential stress and the critical circumferential stress is used to determine if the crack should accelerate or decelerate. The change in crack velocity is assumed proportional to the difference between the stresses,

$$\dot{v} = A\left[\frac{\sigma_\theta^{\max} - \sigma_{\theta_D}^{\max}}{\sigma_{\theta_D}^{\max}}\right], \tag{11}$$

or in incremental form,

$$\Delta v = A\left[\frac{\sigma_\theta^{\max} - \sigma_{\theta_D}^{\max}}{\sigma_{\theta_D}^{\max}}\right]\Delta t_{n+1/2}, \tag{12}$$

where A is a constant that controls the time period over which the velocity changes. A value of $A = c_R/0.25 \times 10^{-6}$ sec is used in the present calculations and gives good results; however, experiments

on crack tip acceleration could provide a more physically meaningful value. The behavior of this constant can be evaluated after an analysis by examining how well the calculated stress intensities remain on the specified $K_{ID}(v)$ curve.

To aid in staying on this curve, a predictor using the current slope of the $K_{ID}(v)$ curve is added to Eq. (12)

$$\Delta v = A \left[\frac{\sigma_\theta^{\max} - \sigma_{\theta_D}^{\max} - \dfrac{\sigma_{\theta_D}^{\max}}{\partial v} \Delta v}{\sigma_{\theta_D}^{\max}} \right] \Delta t_{n+1/2}\,, \tag{13}$$

This predictor recognizes that increasing velocity can change the critical stress intensity. Solving for Δv, we obtain

$$\Delta v = \left[1 \Big/ \left(1 + \frac{A}{\sigma_{\theta_D}^{\max}} \frac{\partial \sigma_\theta^{\max}}{\partial v} \Delta t_{n+1/2} \right) \right] \left[A \frac{(\sigma_\theta^{\max} - \sigma_{\theta_D}^{\max})}{\sigma_{\theta_D}^{\max}} \right] \Delta t_{n+1/2}\,. \tag{14}$$

Equation (14) allows us to increment the crack velocity in the same manner that the accelerations were used to increment the nodal velocities. Crack arrest occurs when the new velocity is less than or equal to zero.

This algorithm is different from others in the literature (Jung, Ahmad, Kanninen and Popelar 1981; Nishioka and Atluri 1980a) in that it does not directly force the crack velocity to lie on the $K_{ID}(v)$ curve. Instead, this occurs naturally as a consequence of the fracture process. The algorithm encounters no difficulty with a flat (constant) $K_{ID}(v)$ curve.

The crack tip propagates in the direction of maximum circumferential stress. The crack tip is moved every time step.

4.3 Transfer of data between meshes when the crack tip is moving

Because of inertia, the dynamic solution represents an evolving history, and whenever the mesh is changed, this history must be preserved. This is accomplished by transferring data from the old mesh to the new mesh.

Three situations arise when regard to transferring data and incrementing in time:

(1) The first case is when the mesh is not changing, but the solution is being incremented in time. This is the standard finite element situation and is represented by Eq. (9). For this case, time derivatives are used to increment the solution.

(2) The second case occurs when the solution is not being incremented in time but when the mesh is being changed, for example, when remeshing to correct element distortion. In this case, spatial derivatives are used to obtain nodal values at the new node positions.

(3) The last case occurs when both the solution is being incremented in time and the coordinates of the nodes are being changed. Both time and spatial derivatives are necessary to update nodal quantities. This case occurs when the crack is propagating.

During the solution, displacements (and velocities and stresses) are functions of position and time. As an example, for the X displacement,

$$u_X = u_X(X, Y, t) \tag{15}$$

The time derivative of the displacement is,

$$\mathrm{d}u_X/\mathrm{d}t = (\partial u_X/\partial X)(\partial X/\partial t) + (\partial u_X/\partial Y)(\partial Y/\partial t) + (\partial u_X/\partial t) \tag{16}$$

or in incremental form,

$$\Delta u_X = (\partial u_X/\partial X)\Delta X + (\partial u_X/\partial Y)\Delta Y + (\partial u_X/\partial t)\Delta t\,. \tag{17}$$

Equation 17 is a more general form of Eq. 9, which describes the central difference scheme.

Spatial derivatives in Eq. (17) could be evaluated and used to find the change in nodal velocity. An equivalent way to do this incrementally is to save the mesh data for the current time and then

to interpolate the current mesh data to the new nodal position. Subtracting the nodal value at the old position from the value at the new position gives the increment in displacement due to moving the node,

$$(\partial u_X/\partial X)\Delta X = u_X|_{X+\Delta X} - u_X|_X. \tag{18}$$

This approach is more natural for finite element analysis where we readily have the shape functions available for interpolating mesh data. The time derivative term of Eq. (17) is calculated using the standard time integration scheme. Then, for the nodes that have moved, the change in displacements due to the spatial gradients is added. A similar procedure is used to update velocities, but with the singular velocities substracted before the interpolation and then added in after interpolation. Nodal masses are recalculated each time step.

It is important to note that there is no attempt to force the stress intensity to be a specified value in the next time step. The stress intensities follow from displacement correlation with the updated nodal displacements.

4.4 Moving the crack tip and automatic remeshing

Using the relations developed in Sect. 4.2, the crack tip node and corresponding quarter-point nodes are moved in each time step. This process is illustrated in Fig. 3 for straight and curving cracks. As the tip moves, a point is reached where the mesh becomes excessively distorted. This distortion both introduces errors into the finite element calculation and causes the time step to drop. Since the time step is tied to the element size, a major requirement for the remesh scheme is that it generate new elements that are of similar size to the elements in the vicinity of the crack tip. This means an element splitting algorithm is not satisfactory. Instead, a scheme was chosen where elements around the crack tip are deleted and new ones generated in the local region. Fig. 4 illustrates the remesh process, for which the steps are:

(1) Using a radius based on local element size, a center for remeshing is defined by projecting ahead of the crack tip. This projection allows the crack to propagate about one element length before remeshing is again necessary (Fig. 4b).

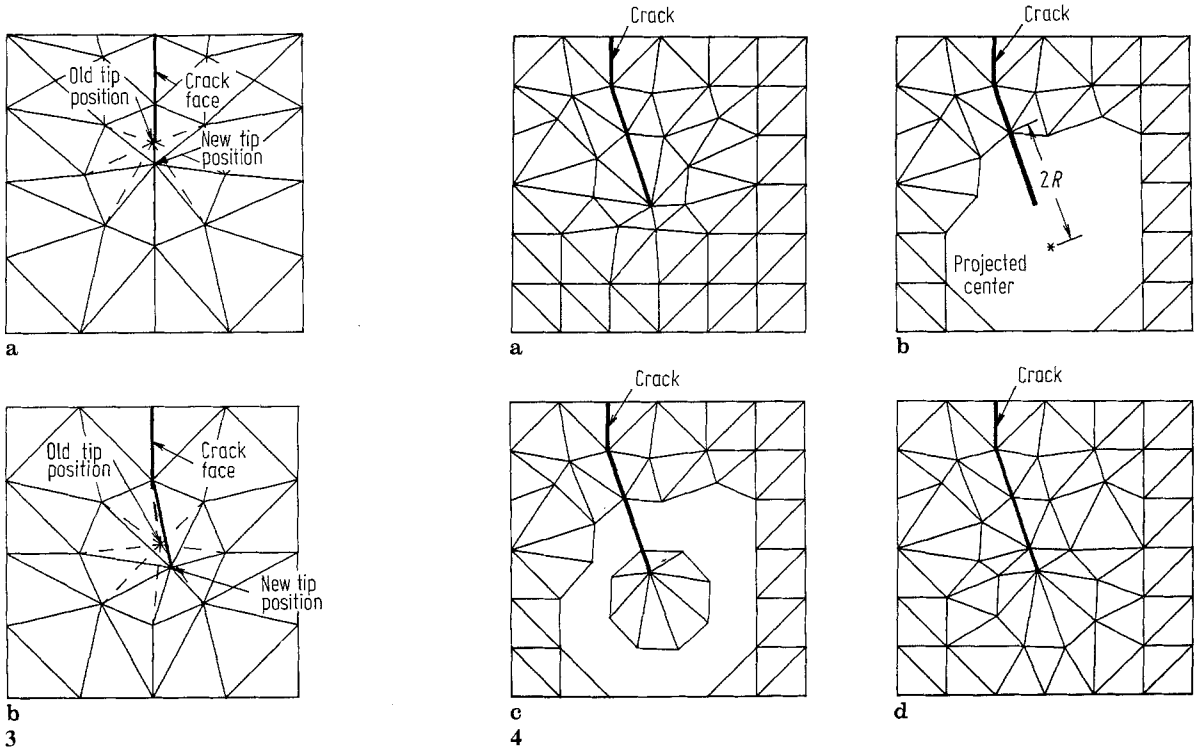

Figs. 3 and 4. 3a,b Method used to move crack tip in mesh; **a** straight crack; **b** curving crack. **4a–d** Automatic remeshing around crack tip; **a** before remeshing; **b** after deleting elements; **c** quarter point elements added; **d** new mesh

(2) All elements within a distance of twice the radius are deleted (Fig. 4b). If necessary, the boundary is smoothed. Data is saved for all the deleted elements.

(3) A rosette of quarter-point elements is added around the crack tip (Fig. 4c).

(4) If needed, nodes are added to the annulus between the quarter-point elements and the boundary.

(5) The annulus is filled with elements (Fig. 4d). The algorithm used is the modified Suhara-Fukuda algorithm described by Shaw and Pitchen (1978).

(6) Data is transferred from the old mesh to the new mesh. Since the problem is fixed in time and only the mesh is being changed, the shape functions are used to interpolate the velocities and displacements of the new nodes. In general, element stresses and strains would also need to be interpolated; however, since an elastic material is assumed, the new values can be calculated directly from the displacements. In addition, nodal masses are recalculated to correspond to the new mesh.

Experience shows this algorithm to be quite reliable. If problems are encountered, the user is given the option of interactively remeshing.

Deleting and adding elements and nodes implies the data describing the problem must be changed. The data base uses a connectivity list for each element and nodal positions for each node. To prevent the data base from expanding as the problem progresses, lists of "dead" elements and "dead" nodes are maintained. When new elements are added, they are put in the positions of the "dead" elements. If no "dead" elements are available, the new elements are added to the end of the element list. The same is done for nodes. This procedure keeps the size of the data base about constant. The ability to add and delete elements without regard for bandwidth (because of the explicit scheme) greatly simplifies the bookkeeping process.

4.5 User interaction

Interactive computer graphics is essential for reliable analysis of mixed-mode dynamic fracture. Because elements are continuously being added and deleted, the topology of the problem is always changing. It is difficult to develop algorithms that allow arbitrary remeshing in all instances of crack propagation. Instead, the approach taken has been to develop a remeshing algorithm that handles most cases, but allows the user to modify the mesh when necessary (such as initiating a crack from a surface). Interactive graphics makes this user control possible.

Interactive graphics also gives the analyst powerful tools with which to evaluate intermediate and final results. Examples include the use of line plots to evaluate convergence by examining stress continuity across elements and the use of projected stress plots to follow wave propagation through the structure.

5 Verification problems

5.1 Sudden appearance of a stationary crack in an infinite medium

The first verification problem is the sudden appearance of a crack in a body under an initial state of stress. By superposition, this is equivalent to a stationary crack subjected to a step plane wave (either dilational or shear) traveling normal to the crack face. The problem has been solved analytically by Thau and Lu (1971). Their solution was obtained using the generalized Wiener-Hopf technique and is valid from the time the wave reaches the crack until the time required for a dilatational wave to travel from one tip to the other and return (two P-wave crack-width transit times).

Finite element solutions were obtained with two meshes: a fine mesh shown in Fig. 5 (only the upper half of the mesh is shown) and a coarse mesh using the same pattern but with one-quarter the number of elements. Material properties were $E = 30 \times 10^6$ lb/in^2, $\nu = 0.25$, and $\varrho = 0.0008$ lb-sec^2/in^4. This results in wave speeds $c_1 = 2.1213 \times 10^5$ in/sec, $c_2 = 1.2247 \times 10^5$ in/sec, and $c_R = 1.1126 \times 10^5$ in/sec. The calculation was performed by specifying and initial stress of $\sigma_Y = 1000$ lb/in^2 for the Mode *I* analysis and $\sigma_{XY} = 1000$ lb/in^2 for the Mode *II* case. Plane strain conditions were assumed.

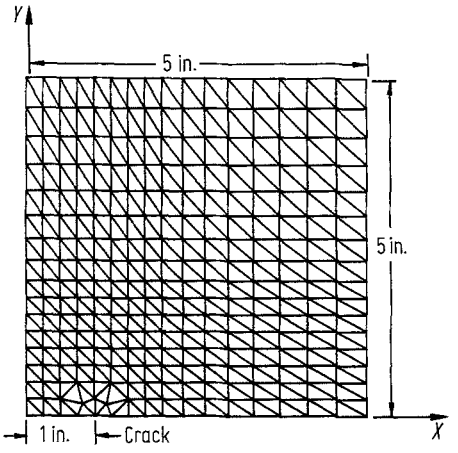

Fig. 5. Mesh used for sudden appearance of crack in an infinite region

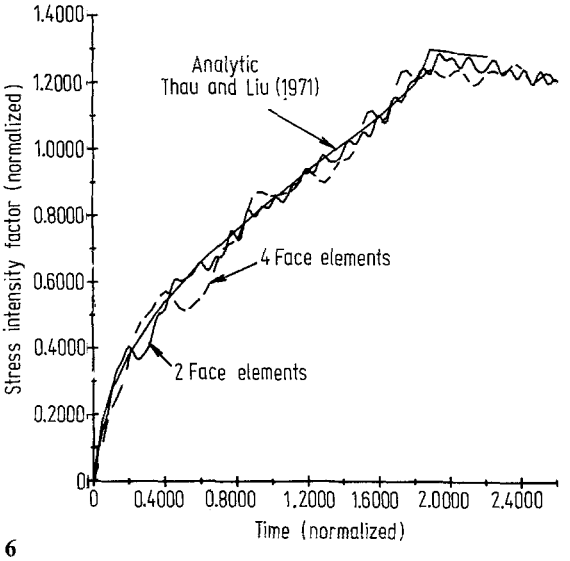

6

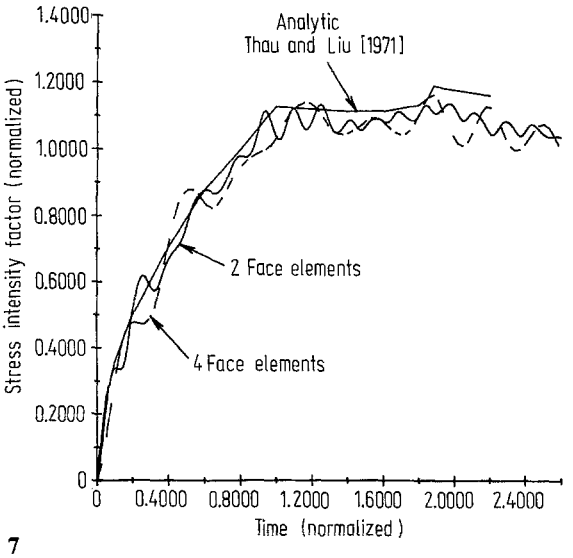

7

Figs. 6 and 7. 6 Mode *I* Loading. 7 Mode *II* Loading

Results for the Mode *I* loading are shown in Fig. 6. In this plot, time is normalized by the time for a dilatational wave to traverse the length of the crack, and the stress intensities are normalized by the static value. The correlation between finite element results and analytical results is good. The finite element results show some oscillation, with the finer mesh giving improved results.

Fig. 7 shows corresponding results for shear loading. For this case, the correlation of finite element results with analysis is not as good as for the Mode *I* case, but still satisfactory.

5.2 Propagating crack in an infinite medium

In previous studies, verification of crack propagation calculations has been performed by approximating steady state solutions or by approximating Broberg's solution for a crack propagating from an initially zero length. Because of these approximations, the comparisons are uncertain. By using Freund's solution (Eq. 1) for a crack propagating in an infinite medium, we can develop a simple verification problem with which numerical results can be unambiguously compared.

Using Eq. (1), analytic solutions can be obtained either for the case where the crack velocity history is specified and the stress intensity is calculated ("generation" studies) or for the case where the stress intensity is specified and the crack velocity history is obtained ("application" studies). The former is a direct application of Eq. (1), while the latter involves an integration of the crack velocity.

Eq. (1) was derived for an infinite body but applies to a finite body until the arrival of reflected waves.

Freund's solution requires as input the initial static stresses on the crack axis ahead of the crack. The simplest problem for which an analytic solution is available is that for a static semi-infinite crack in an infinite body. For this problem, the static asymptotic $1/\sqrt{r}$ solution (Eqs. (2) and (3) with zero velocity) can be used to obtain traction boundary conditions which make the finite body act as though it is infinite. If this is done, the stresses ahead of the crack given by the asymptotic solution can be used as input to Freund's analysis to calculate $K_S(a)$. For this particular problem, the parameter $K_S(a)$ is constant and equal to the initial static value, independent of crack length. As a consequence, if a constant crack velocity is specified, the analytic solution is a constant dynamic stress intensity (Eq. (1)), or inversely, if a constant critical stress intensity is specified, the resulting crack velocity will be constant.

Figure 8 shows the mesh used to model the "infinite" problem. Results will be presented for a fine mesh and a course mesh. Both used the same mesh pattern, but the diameter was 2.5 inches for the fine mesh and 5.0 inches for the coarse mesh. Traction boundary conditions on the outer surface corresponding to a static stress intensity of $K_I = 1000$ psi-in$^{1/2}$ were applied. Material properties were the same as for the previous example. The problem was first brought to initial static equilibrium and then either the crack velocity or critical stress intensity was specified. When the velocity was specified, the critical stress intensity was calculated as the dependent variable. When the critical stress intensity was specified, the crack velocity was calculated.

In the first analysis, the crack velocity was specified to be 0.4 of the Rayleigh wave speed (crack velocity = 44504 in/sec). Figure 9 shows the crack tip opening displacement profiles at the initial static condition and after the crack has propagated. The stress intensities during the propagation are shown in Fig. 10. The calculated initial static equilibrium stress intensity is 987 psi-in$^{1/2}$, while the exact value is 1000 psi-in$^{1/2}$. Based on Freund's analysis, the stress intensity corresponding to the specified velocity should be 725 psi-in$^{1/2}$.

The results for a specified stress intensity are shown in Fig. 11. The specified stress intensity is 725 psi-in$^{1/2}$, corresponding to a velocity of 4450 in/sec. Figure 11 b shows the attempt of the finite element solution to maintain the calculated stress intensity on the specified stress intensity curve. This calculation is a more severe test of the algorithm's capability than the analysis with a specified velocity, since errors in the stress intensity are magnified when calculating the velocity (Sect. 4.2). Finally, Fig. 12 shows the energy partitioning during crack propagation with a specified velocity. As it should, the total energy remained nearly constant. The energy balance for the analysis with a specified stress intensity was essentially identical.

After each remeshing the results show a short transient in stress intensity and crack velocity, with the magnitudes of the errors about the same for either the fine or coarse mesh. Remeshing

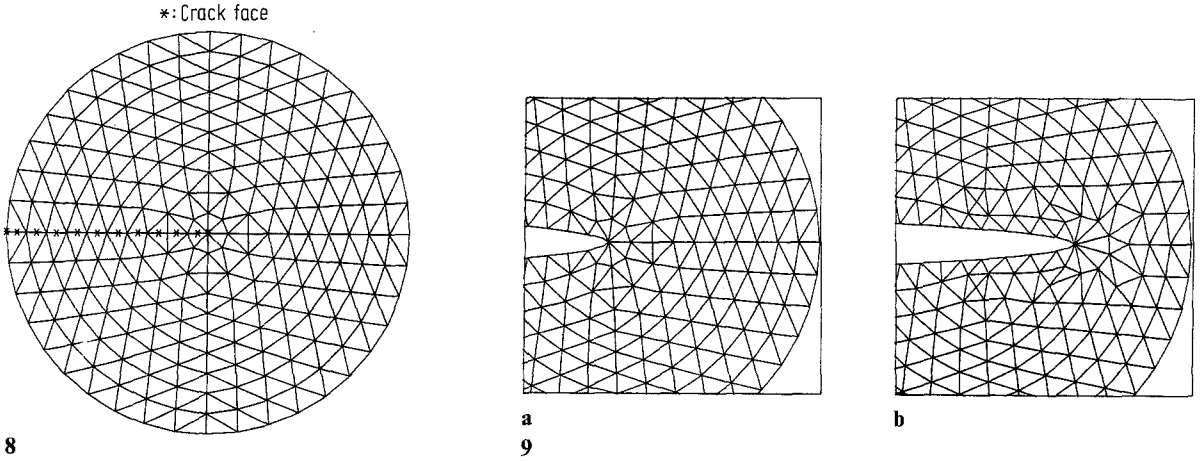

8 9

Figs. 8 and 9. 8Mesh used for analysis of "infinite" body. **9 a, b** Displaced mesh plots with velocity specified (magnification = 4000); **a** displacements at static equilibrium; **b** after 25×10^{-6} sec.

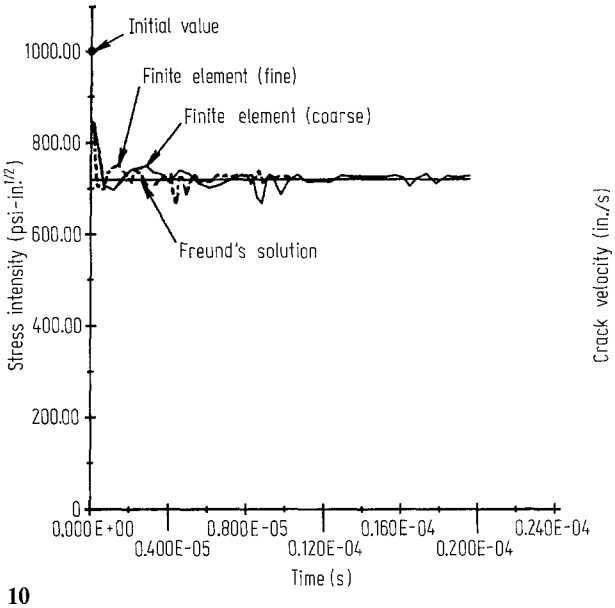

10

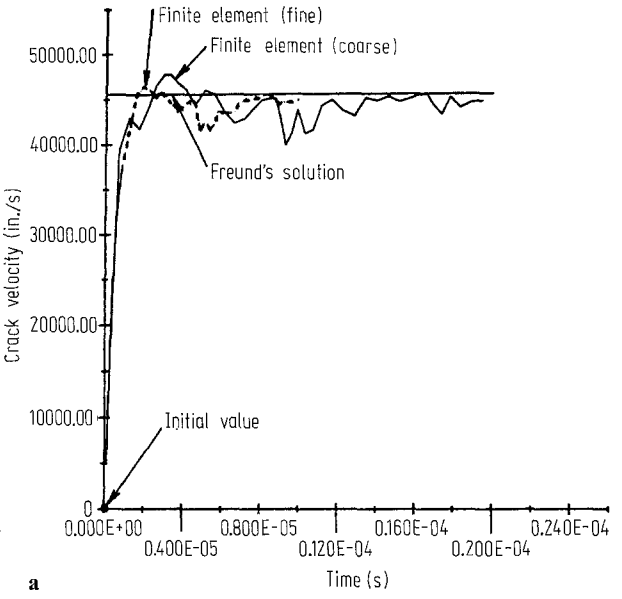

a

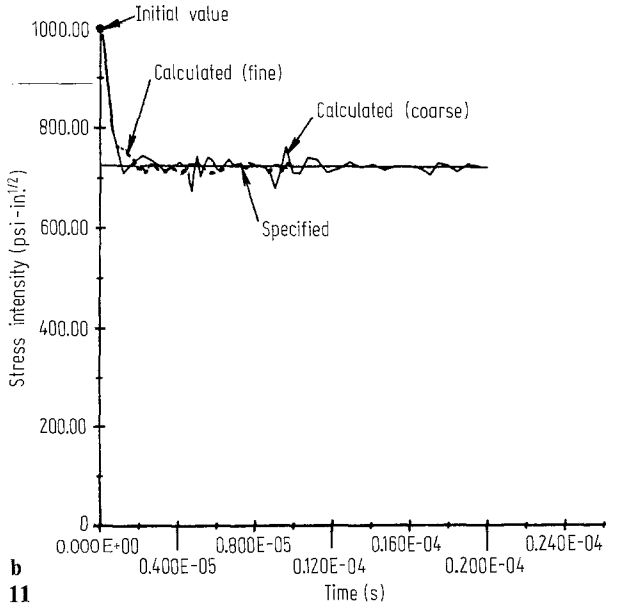

b

11

Figs. 10 and 11. "Infinite" problem **10** with velocity specified stress intensity following crack initiation; **11 a, b** with K_{ID} specified; **a** calculated crack velocity; **b** stress intensity as a function of crack velocity

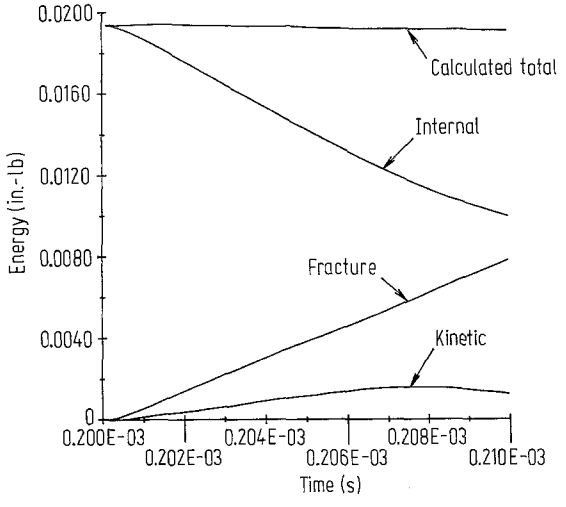

Fig. 12. Energy balance for "Infinite" problem

changes the finite element approximating functions around the tip and thus introduces some error. Since the quarter-point node displacements are used to calculate the stress intensity for both meshes, the physical point used for the evaluation is closer to the crack tip in the fine mesh. Thus the magnitude of the error is about the same for both meshes. The results could probably be improved by evaluating the stress intensity using displacements at a fixed radius rather than a radius that changes with the mesh.

6 Analysis of crack curving under biaxial loading

To demonstrate the application of the model to a mixed-mode problem, we will examine experiments performed by Dadkhah (1984) and reported by Hawong, Kobayashi, Dadkhah, Kang and Ramulu (1985). In the experiments, a centrally-cracked Homalite 100 plate was subjected to biaxial loads. Depending on the biaxial load ratio, the fracture propagated in different directions. Measured data included the load on the plate and photographs from a 16 spark-gap camera. This allowed the stress intensity during propagation and crack position to be obtained directly.

Figure 13 shows the test specimen which was loaded by four hydraulic cylinders attached by grip plates and miscellaneous hardware that totaled 7.4 lb weight for each of four cylinders. The load was applied rapidly over a time of about 40×10^{-6} sec, as shown in Fig. 14. The test which will be analyzed had a biaxial load ratio of 1.6. That is, the load in the X direction was 1.6 times the load in the Y direction. The crack was initially aligned along the X axis, so if the crack deviated from the symmetry line, there was a strong tendency for the crack to turn. Although the test specimen was loaded as symmetrically as possible, the initial crack propagation angle was 5 degrees off the symmetry axis. The reason for this unsymmetric response is not known.

Coarse and fine meshes were used in the calculations, with the fine mesh shown in Fig. 15. Plane stress assumptions were used, with the density of the outer edge elements increased to account for the mass of the loading fixture. In the analysis some initial asymmetry must be supplied or the crack will propagate symmetrically. The asymmetry was supplied by orienting the crack tip elements at initial angles of 5 or 10 degrees. The thickness of the specimen was 0.646 inches. Material properties of Homalite 100 are $E = 0.619 \times 10^6$ lb/in^2, $\nu = 0.357$, and $\varrho = 0.000112$ lb-sec^2/in^4. The properties give plane stress wave speeds of $c_1 = 79600$ in/sec, $c_2 = 45100$ in/sec, and $c_R = 41600$ in/sec. The specified K_{ID} (v) curve is shown in Fig. 16. This data was obtained independently from the present test (Metcalf and Kobayashi, 1986).

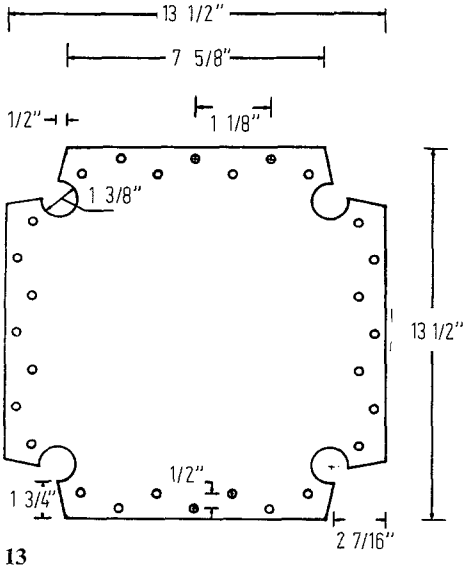

13

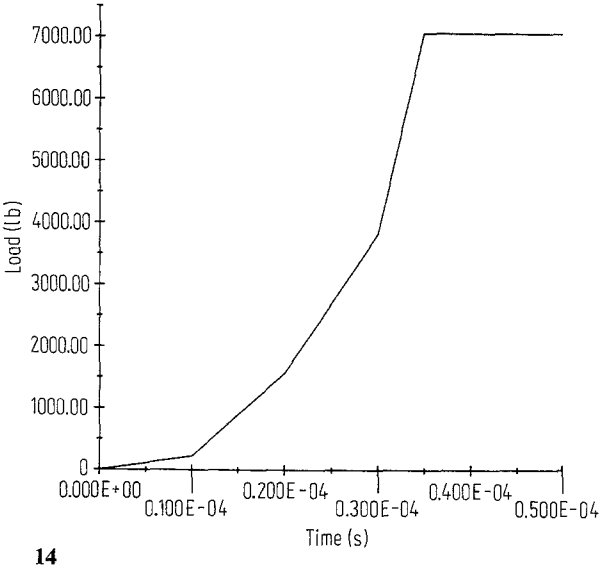

14

Figs. 13 and 14. 13 Cruciform test specimen (Dadkhah 1984); **14** loading on biaxially loaded specimen

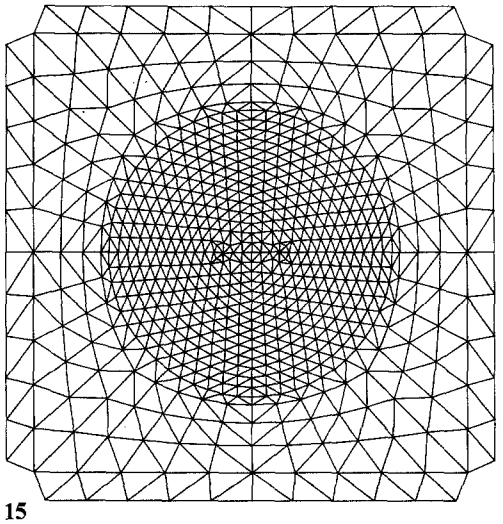

15

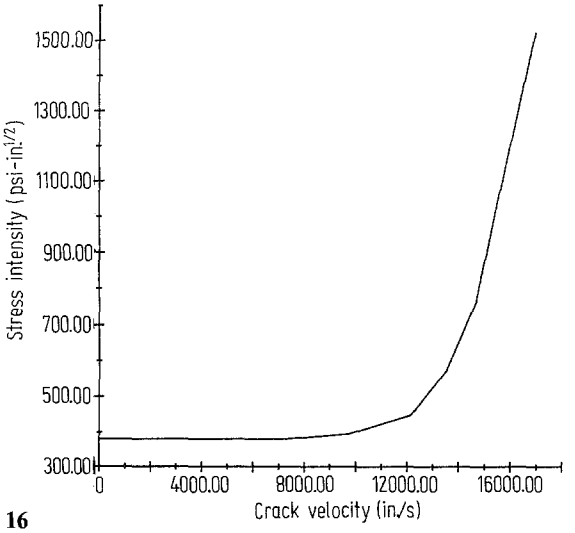

16

Figs. 15 and 16. 15 Fine mesh of biaxially loaded specimen; **16** specified $K_{ID}(v)$ curve for Homalite 100

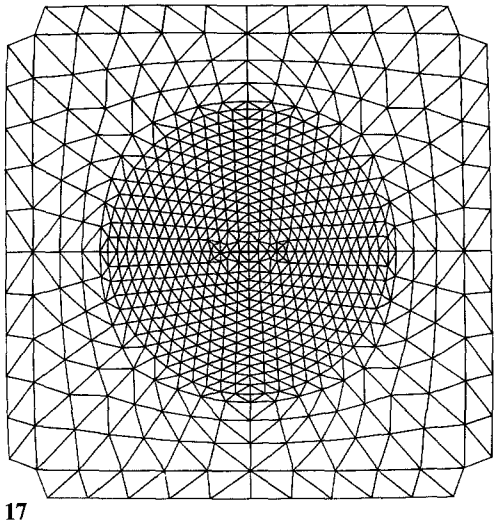

17

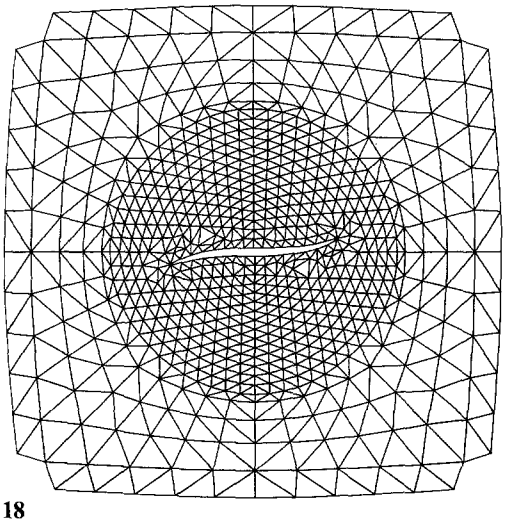

18

Figs. 17 and 18. Calculated displacements **17** at 100×10^{-6} sec; **18** at 200×10^{-6} sec (magnification = 30)

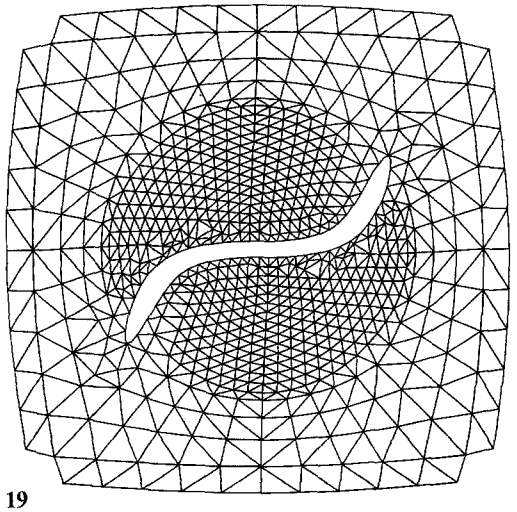

19

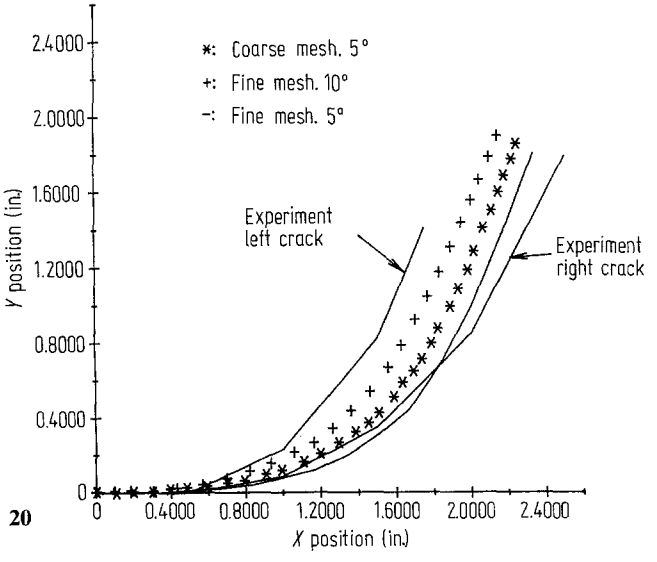

20

Figs. 19 and 20. 19 Calculated displacements at 300×10^{-6} sec (magnification = 30); **20** Comparison of calculated and observed crack paths

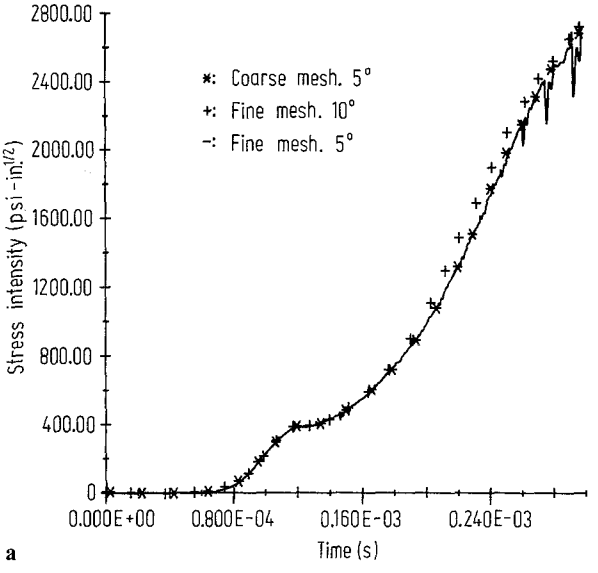

a

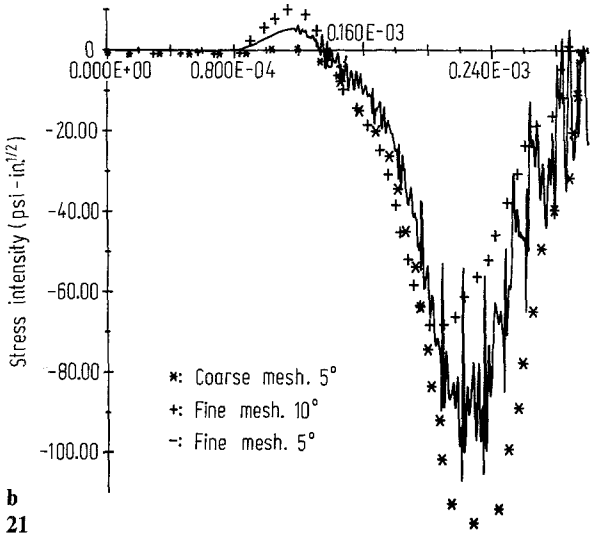

b

21

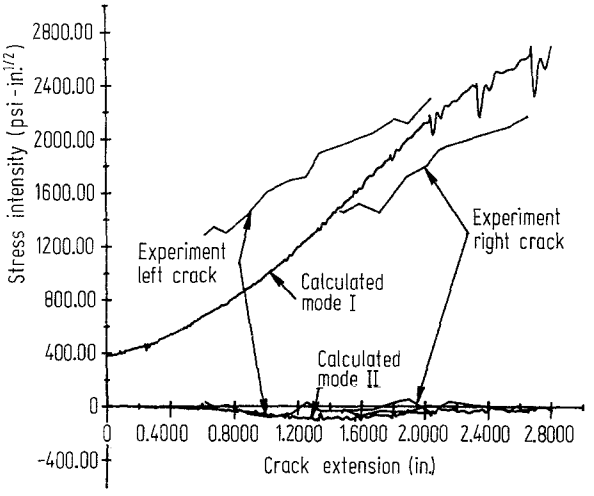

22

Figs. 21 and 22. 21 a, b Calculated stress intensity factors; **a** Mode *I* stress intensity; **b** Mode *II* stress intensity; **22** Comparison of calculated and observed stress intensity factors

Displacement results are shown in Fig. 17 through 19 for the fine mesh with the crack tip elements given an initial angle of 5 degrees. Figure 20 compares the calculated crack paths to experiemental data. The path is relatively insensitive to the change in initial angle from 5 to 10 degrees. Agreement between the computed and experimentally observed trajectories is good, with the calculations falling between the observed values for the left and right cracks.

The computed stress intensities as a function of time are shown in Fig. 21. One item of significance is the ratio of Mode *II* to Mode *I* stress intensity. The Mode *II* stress intensity is about a factor of ten lower than the Mode *I* value. This confirms that a relatively small value of Mode *II* is sufficient to turn a crack significantly. A comparison of calculated and measured stress intensities is given in Fig. 22. The calculated values are again bounded by measured results for the left and right sides of the crack, with the Mode *II* components being much smaller than the Mode *I* values.

7 Conclusions

This paper has presented a finite element model of mixed-mode dynamic fracture where discrete cracks are allowed to propagate in direcitons not chosen a priori. Important features are the use of triangular elements with quadratic shape functions, explicit time integration, and interactive com-

puter graphics. These features make it possible to reliably remesh as the crack propagates and allow the singularity at the crack tip to be modeled. The algorithms for predicting crack velocity and propagation direction allow a general specification of the critical stress intensity.

Verification of the model was performed by analyzing two problems: the sudden appearance of a stationary crack in a stressed body and the propagation of a crack in an infinite body. It is recommended that this infinite body problem, for which an exact analytical solution is available, be used for verification of numerical models.

The analysis of the biaxially loaded plate illustrates the application of the model to mixed-mode propagation. Good correlation was obtained with the available data for crack trajectory and observed stress intensities. This analysis demonstrates that only a small Mode *II* component is sufficient to significantly curve the crack path.

These results (and others Swenson (1985); Swenson and Ingraffea (1986)) show that the relatively simple assumptions used for propagation criteria are sufficient for a relatively broad range of dynamic fracture problems. These criteria are the use of maximum circumferential stress for the crack propagation direction and the use of a $K_{ID}(v)$ curve for critical stress intensity.

Acknowledgements

The authors are grateful for valuable discussions with Professors A. Ruina and H. Hui, at the Theoretical and Applied Mechanics Department of Cornell University. Dr. W. Gerstle provided guidance on interactive computer graphics. Development of the program was done at the Computer Graphics Laboratory, Cornell University. The first author was supported in his studies by Sandia National Laboratories, Albuquerque, New Mexico. Partial funding was provided by National Science Foundation Grant Number 8351914.

References

Achenbach, J.D.; Bazant, Z.P. (1975): Elastodynamic near-tip stress and displacement fields for rapidly propagating cracks in orthotropic materials. J. Appl. Mech. 18/1, 1–22

Atluri, S.N.; Nishioka, T.N. (1985): Numerical studies in dynamic fracture mechanics. Int. J. Fracture 27, 245–261

Barsoum, R.S. (1977): Triangular quarter-point elements as elastic and perfectly-plastic crack tip elements. Int. J. Num. Meth. for Eng. 9, 495–507

Bathe, K.-J. (1982): Finite element procedures in engineering analysis. New Jersey: Prentice-Hall

Belytschko, T.; Hughes, T.R. (eds.) (1983): Computational methods for transient analysis. Amsterdam: North-Holland

Broberg, K.B. (1951): The moving griffith crack. Phil. Mag. 42, 739–750

Chen, Y.M.; Wilkins, M.L. (1977): Numerical analysis of dynamic Crack Problems. Elastodynamic crack problems. Leyden: Noordhoff

Dadkhah, M.S. (1984): Dynamic fracture under the influence of biaxial state of stress. Master's Thesis, Mech. Eng., University of Washington

Freund, L.B. (1972a): Crack propagation in an elastic solid subjected to general loading-I. Constant rate of extension. J. Mech. Phys. Solids 20, 129–140

Freund, L.B. (1972b): Crack propagation in an elastic solid subjected to general loading-II. Non-uniform rate of extension. J. Mech. Phys. Solids 20, 141–152

Freund, L.B. (1973): Crack propagation in an elastic solid subjected to general loading-III. Stress wave loading. J. Mech. Phys. Solids 21, 47–61

Freund, L.B. (1974): Crack propagation in an elastic solid subjected to general loading-III. Stress wave loading. J. Mech. Phys. Solids 22, 137–146

Freund, L.B.; Clifton, R.J. (1974): On the uniqueness of plane elastodynamic solutions for running cracks. J. Elasticity 4/4 293–299

Hawong, J.S.; Kobayashi, M.S.; Dadkhah, M.S.; Kang, S.J.; Ramulu, M.: Dynamic crack curving and branching under biaxial loading. Office of Naval Res., Tech. Rpt. No. UWA/DME/Tr-85/50

Henshell, R.D.; Shaw, K.G. (1975): Crack tip finite elements are unnecessary. Int. J. Numer. Meth. in Eng. 12, 93–99

Jung, J.; Ahmad, J.; Kanninen, M.F.; Popelar, C.H. (1981): Finite element analysis of dynamic crack propagation. Failure prevention and reliability, Proc. of the design engineering technical conference sponsored by the reliability stress analysis and failure prevention committee, the design engineering division of ASME, Hartford, Conn.

Key, S.W.; Beisinger, Z.E.; Krieg, R.D. (1978): Hondo II – A finite element computer program for the large deformation dynamic response of axisymmetric solids. SAND78-0422, Sandia National Laboratories, Alburquerque, NM.

Kobayashi, A.S.; Emery, A.S.; Mall, S. (1976): Dynamic-finite-element and dynamic-photoelastic analyses of two fracturing homalite-100 plates. Exper. Mech. 16/9, 321–328

Koh, H.M.; Haber, R.B. (1986): A mixed Eulerian-Lagrangian model for the analysis of dynamic fracture. UILU-ENG-86-2003, University of Illinois, Urbana, Ill.

Metcalf, J. T.; Kobayashi, T. (1986): Comparison of crack behavior in homalite 100 and araldite B. Crack arrest methodology and applications, ASTM STP 711, Hahn, G. T.; Kanninen, M. F. (eds.), Amer. Soc. of Testing and Materials, 128–145
Nilsson, F. (1972): Dynamic stress-intensity factors for finite strip problems. Int. J. Fracture Mechanic 8/4, 403–411
Nishioka, T.; Atluri, S. N. (1980a): Numerical modeling of dynamic crack propagation in finite bodies, by moving singular elements – part 1: Formulation. J. Appl. Mech. 47, 570–576
Nishioka, T.; Atluri, S. N. (1986b): Numerical modeling of dynamic crack propagation in finite bodies by moving singular elements – part 2: Results. J. Appl. Mech. 47, 577–582
Nishioka, T.; Atluri, S. N. (1983): Path-independent integrals, energy release rates and general solutions of near-tip fields in mixed-mode dynamic fracture mechanics. Eng. Frac. Mech. 18/1, 1–22
Radok, J. R. M. (1956): On the solution of problems of dynamic plane elasticity. Q. Appl. Mathem. 14, 289–298
Rosakis, A. J.; Duffy, J.; Freund, L. B. (1984): The determination of dynamic fracture toughness of AISI 4340 steel by the shadow spot method. J. Mech. Phys. Solids 31/3, 251–260
Rossmanith, H. P. (1983): How mixed-mode crack propagation? A dynamic photoelastic study. J. Mech. Phys. Solids 31/3, 251–260
Sih, G. C.; Chen, E. P. (1977): Cracks moving at constant velocity and acceleration. Elastodynamic crack problems. Leyden: Noordhoff
Shaw, R. D.; Pitchen, R. G. (1978): Modifications to the Suhara-Fukuda method of network generation. Int. J. Numer. Meth. Eng. 12, 93–99
Swenson, D. V. (1986): Derivation of the near-tip stress and displacement fields for constant velocity crack without using complex functions. Tech. note in Eng. Fract. Mech. 18/1, 1–22
Swenson, D. V. (1985): Modeling mixed-mode dynamic crack propagation using finite elements. Dept. Struct. Eng. Rpt. No. 85-10, Civil and Environmental Engineering, Cornell University, Ithaca, NY
Swenson, D. V. (1986): On using combined experimental/analysis to generate dynamic critical stress intensity data. Presented at 19th national symposium on fracture mechanics, June 30–July 2, San Antonio, Texas. ASTM STP (to be publ.)
Thau, S. A.; Lu Tsin-Ywei (1971): Transient stress intensity for a finite crack in an elastic solid caused by a dilatational wave. Int. J. Solids and Struct. 7, 731–750
Valliappan, S.; Murti, V. (1985): Automatic remeshing technique in quasi-static and dynamic crack propagation. Proc. of the NUMETA 1985 Conference, Swansea, January 7–11
Yoffe, E. H. (1951): The moving griffith crack. Philosophical Magazine 42, 739–750

Communicated by S. N. Atluri, April 3, 1987